

A Finite Element 3D Stokes Ice Sheet Dynamics Model with Enhanced Local Mass Conservation

Lili Ju

Department of Mathematics
University of South Carolina

Collaborators:

W. Leng, T. Cui (CAS), T. Zhang (USC)

M. Gunzburger (FSU), S. Price (LANL)

SIAM Conference on Computational Science & Engineering
March 14, 2015



Outline

- 1 Background
- 2 Mathematical Modeling of Ice Sheet Flow
- 3 Computational Ice Sheet Model - Discretization and Solution
- 4 Numerical Experiments
 - Tests of the Stokes ice dynamics solver
 - Tests of thermo-mechanically coupled ice sheet evolution
- 5 Conclusions



Background

- Among several approaches for computational modeling of land-ice evolution, the **nonlinear 3D Stokes** model is generally accepted as the gold standard for modeling the flow of ice sheets.
- A nonlinear 3D Stokes ice-sheet model requires the integration of effective meshing strategies, accurate discretization schemes, couplers for momentum, energy and mass balance components, efficient and scalable parallel solvers.
- The current widely-used reduced models: zeroth-order models ([shallow-ice](#), [shallow-shelf](#)) and first-order models ([L1L2](#), [Blatter-Pattyn](#)) are all obtained as reduced forms of the 3D Stokes model by means of scaling analyses, but, with an attendant loss of fidelity.
- A finite element full-Stokes model: [Elmer](#) [Le Meur and *et. al.*, 2004]
- The PISCEES project (Predicting Ice Sheet and Climate Evolution at Extreme Scales, 2012-2017) funded by US DoE Office of Science.
 - [FELIX](#) – Finite Element Land Ice eXperiments
Our task: FELIX-Stokes.



Outline

- 1 Background
- 2 Mathematical Modeling of Ice Sheet Flow**
- 3 Computational Ice Sheet Model - Discretization and Solution
- 4 Numerical Experiments
 - Tests of the Stokes ice dynamics solver
 - Tests of thermo-mechanically coupled ice sheet evolution
- 5 Conclusions



Ice Sheet Dynamics: 3D Stokes Equations

The dynamical behavior of the ice sheet is modeled by the nonlinear Stokes equations for an incompressible viscous fluid in a low Reynolds-number flow over the time interval $[0, t_{max}]$ and in the three-dimensional spatial domain Ω_t occupied by the ice sheet:

$$\begin{aligned}\rho \frac{d\mathbf{u}}{dt} &= \nabla \cdot \boldsymbol{\sigma} + \rho \mathbf{g} && \text{in } \Omega_t \times [0, t_{max}], \\ \nabla \cdot \mathbf{u} &= 0 && \text{in } \Omega_t \times [0, t_{max}],\end{aligned}$$

where

- $\mathbf{u} = (u_1, u_2, u_3)^T$ denotes the velocity,
- $\boldsymbol{\sigma}$ is the full stress tensor,
- ρ is the density of ice,
- $\mathbf{g} = (0, 0, -g)$ denotes the gravitational acceleration,
- $\Omega_t = \{(x, y, z) \mid b(x, y) \leq z \leq s(x, y, t) \text{ for } (x, y) \in \Omega_H, t \in [0, t_{max}]\}$.



Instantaneous Momentum Balance

- The full stress tensor σ can be decomposed in terms of deviatoric stress τ and the static pressure p as

$$\sigma = \tau - p\mathbf{I}$$

where $p = -\frac{1}{3}\text{tr}(\sigma)$.

- Assume that the entire material derivative $\frac{d\mathbf{u}}{dt}$ is neglected because the time scale of variations of the velocity and pressure fields is large.

\implies The momentum balance equation

$$-\nabla \cdot \tau + \nabla p = \rho \mathbf{g} \quad \text{in } \Omega_t \times [0, t_{max}]. \quad (1)$$

- The strain rate tensor $\dot{\epsilon}_{\mathbf{u}}$ is the function of displacement speed defined as

$$\dot{\epsilon}_{\mathbf{u}} = \frac{1}{2}(\nabla u + \nabla u^T)$$

and the effective strain rate $\epsilon_{\mathbf{u}}$ is defined as $\epsilon_{\mathbf{u}} = \sqrt{\frac{1}{2}\dot{\epsilon}_{\mathbf{u}} : \dot{\epsilon}_{\mathbf{u}}}$.



Constitutive Law

The constitutive law for ice relates the deviatoric stress τ to the strain rate tensor $\dot{\epsilon}_{\mathbf{u}}$ by the generalized Glen's flow law

$$\tau = 2\eta_{\mathbf{u}}\dot{\epsilon}_{\mathbf{u}}$$

with the viscosity

$$\eta_{\mathbf{u}} = \frac{1}{2}A^{-1/n}\epsilon_{\mathbf{u}}^{(1-n)/n},$$

where

- n is the power-law exponent,
- $\eta_{\mathbf{u}}$ is the temperature- and strain rate-dependent rheology coefficient.
- A denotes the deformation rate factor (Glen's flow law), that obeys an *Arrhenius* relation defined by $A = A(T) = a \exp\left(-\frac{Q}{RT}\right)$ where
 - a is an empirical flow constant, Q denotes the activation energy, R the universal gas constant.



Boundary Conditions for Dynamics

- At the top surface Γ_s of the ice sheet, we impose the boundary condition

$$\boldsymbol{\sigma} \cdot \mathbf{n} = -p_{atm} \cdot \mathbf{n} \quad \text{on } \Gamma_s$$

- Along the lateral boundary Γ_ℓ we impose one of three types of boundary conditions: a condition such as the above one (air or water); a zero boundary condition $\mathbf{u} = 0$; or periodic boundary conditions.
- On the bottom surface Γ_b , we set the following conditions:

$$\mathbf{u} = 0 \quad \text{on } \Gamma_{b,fix}$$

which is referred to as the *no-slip* boundary condition and

$$\mathbf{u} \cdot \mathbf{n} = 0 \quad \text{and} \quad \mathbf{n} \cdot \boldsymbol{\sigma} \cdot \mathbf{t} = -\beta^2 \mathbf{u} \cdot \mathbf{t} \quad \text{on } \Gamma_{b,sld}$$

which is referred to as the **Rayleigh friction** boundary condition.

- The **nonlinear Coulomb friction** law could be used too.



Ice Temperature Evolution

The governing equation for the temperature in the ice sheet is given by

$$\rho c \frac{\partial T}{\partial t} + \rho c \mathbf{u} \cdot \nabla T = \nabla \cdot (\kappa \nabla T) + 2\eta_{\mathbf{u}} \dot{\epsilon}_{\mathbf{u}} : \dot{\epsilon}_{\mathbf{u}} \quad \text{in } \Omega_t \times [0, t_{max}], \quad (2)$$

where

- c and κ denote the specific heat capacity and thermal conductivity of ice, that are assumed to be independent of ice temperature.
- Non-steady and advective changes in temperature (the first and second terms on the left-hand side respectively) are balanced by *temperature diffusion* and *internal strain heating* (the first and second terms on the right-hand side respectively).
- Suitable boundary conditions for temperature.



Ice Thickness Evolution

The ice-sheet geometry evolution equation, derived from the *local mass conservation*, is given by

$$\frac{\partial H}{\partial t} = -\nabla \cdot (\bar{\mathbf{u}}H) + m \quad \text{in } \Omega_H \times [0, t_{max}], \quad (3)$$

where

- $H = s - b$ denotes the ice thickness,
- $\bar{\mathbf{u}}$ is the vertically averaged velocity,
- m denotes a source/sink term resulting from the ice sheet surface mass balance (i.e., climate driven accumulation or melting of ice) and basal mass balance (i.e., melting or freezing of ice at the ice-bedrock interface).



Model Parameters and Physical Constants

Symbol	Constant	Value	Unit
ρ	Density of ice	910	kg m^{-3}
g	Acceleration due to gravity	9.81	m s^{-2}
n	Power in Glen's law	3	-
T_0	Triple point of water	273.15	K
G	Geothermal heat flux	4.2×10^{-2}	W m^{-2}
k	Thermal conductivity of ice	2.1	$\text{W m}^{-1}\text{K}^{-1}$
c	Specific heat capacity of ice	2009	$\text{J kg}^{-1}\text{K}^{-1}$
γ	Clausius-Clapeyron gradient	8.66×10^{-4}	K m^{-1}
a	Tuning parameter	3.61×10^{-13} if $T < 263.15$ K 1.73×10^{-13} if $T \geq 263.15$ K	$\text{Pa}^{-3}\text{s}^{-1}$
Q	Activation energy	6.0×10^4 if $T < 263.15$ K 13.9×10^4 if $T \geq 263.15$ K	J mol^{-1}
R	Gas constant	8.314	$\text{J mol}^{-1}\text{K}^{-1}$
	Seconds per year	31556926	



Outline

- 1 Background
- 2 Mathematical Modeling of Ice Sheet Flow
- 3 Computational Ice Sheet Model - Discretization and Solution**
- 4 Numerical Experiments
 - Tests of the Stokes ice dynamics solver
 - Tests of thermo-mechanically coupled ice sheet evolution
- 5 Conclusions

Finite Element Spaces

Let \mathcal{T}_h denote a tetrahedral triangulation of the 3D ice sheet domain Ω_t .

- $P_{0,h}(\mathcal{T}_h)$: the piecewise constant polynomial finite element space.
- $P_{1,h}(\mathcal{T}_h)$: the continuous piecewise linear polynomial finite element space.
- $P_{2,h}(\mathcal{T}_h)$: the continuous piecewise quadratic polynomial finite element space.
- $P_{1+0,h}(\mathcal{T}_h)$ consists of functions in $P_{1,h}(\mathcal{T}_h)$ and $P_{0,h}(\mathcal{T}_h)$.

Then

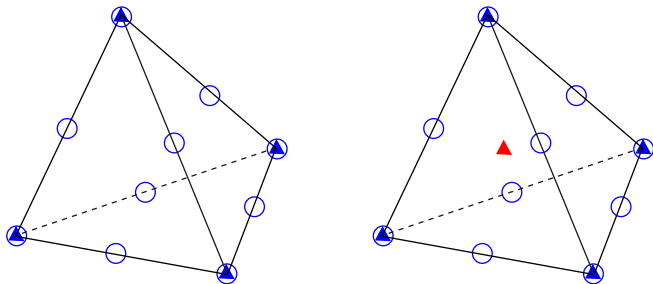
- $(\tilde{\mathbf{P}}_{2,h}(\mathcal{T}_h), P_{1,h}(\mathcal{T}_h))$ is called the **Taylor-Hood element** pair (P2/P1) for velocity and pressure.
- $(\tilde{\mathbf{P}}_{2,h}(\mathcal{T}_h), P_{1+0,h}(\mathcal{T}_h))$ is called the **Enriched Taylor-Hood element** pair (P2/P1+P0) for velocity and pressure.

where

$$\tilde{\mathbf{P}}_{2,h}(\mathcal{T}_h) = \{\mathbf{u}_h \in (P_{2,h}(\mathcal{T}_h))^3 \mid \mathbf{u}_h|_{\Gamma_I \cup \Gamma_{b,\tilde{f}ix}} = 0, (\mathbf{u}_h \cdot \mathbf{n})|_{\Gamma_{b,slid}} = 0\}.$$



Taylor-Hood vs. Enriched Taylor-Hood



The Taylor-Hood element pair (P2/P1) and the enriched Taylor-Hood element pair (P2/P1+P0) where the circles denote the position of velocity DOFs and the triangles that of pressure DOFs.

- The enriched T-H element discretization has about 24% more DOFs than the T-H element discretization ($n_v : n_e : n_t \approx 1 : 7.77 : 6.77$).



FE Discretization of the Stokes Ice Dynamics

- The Taylor-Hood finite element ice dynamics model [Leng et. al, *JGR* 2012]: seek functions $\mathbf{u}_h \in \tilde{\mathbf{P}}_{2,h}(\mathcal{T}_h)$ and $p_h \in P_{1,h}(\mathcal{T}_h)$ such that

$$\begin{cases} \int_{\Omega_t} 2\eta \mathbf{u}_h : \dot{\boldsymbol{\epsilon}} \mathbf{v}_h \, d\mathbf{x} + \int_{\Gamma_{b,slid}} \beta^2 \mathbf{u}_h \cdot \mathbf{v}_h \, ds - \int_{\Omega_t} p_h \nabla \cdot \mathbf{v}_h \, d\mathbf{x} = \rho \int_{\Omega_t} \mathbf{g} \cdot \mathbf{v}_h \, d\mathbf{x}, \\ - \int_{\Omega_t} q_h \nabla \cdot \mathbf{u}_h \, d\mathbf{x} = 0, \end{cases} \quad (4)$$

for all $\mathbf{v}_h \in \tilde{\mathbf{P}}_{2,h}(\mathcal{T}_h)$ and $q_h \in P_{1,h}(\mathcal{T}_h)$.

- The enriched Taylor-Hood finite element ice dynamics model [Leng et. al, *JCP* 2014]: replace $P_{1,h}(\mathcal{T}_h)$ by $P_{1+0,h}(\mathcal{T}_h)$ in (4).
 - The enriched Taylor-Hood finite element model greatly enhances local mass conservation since holds

$$\int_T \nabla \cdot \mathbf{u}_h \, d\mathbf{x} = 0,$$

i.e., exactly **local mass conserved** for any $T \in \mathcal{T}_h$.



Nolinear Solver: Picard Iterations

A direct Picard-type iterative algorithm is to solve the nonlinear system, in which the variables used for evaluation of the velocity-dependent viscosity $\eta_{\mathbf{u}}$ for the j -th step are taken from the $(j - 1)$ -th iteration step of the algorithm as follows:

$$\begin{cases} \int_{\Omega_t} 2\eta_{\mathbf{u}_h^{(j-1)}} \dot{\epsilon}_{\mathbf{u}_h^{(j)}} : \dot{\epsilon}_{\mathbf{v}_h} \, d\mathbf{x} + \int_{\Gamma_{b,slid}} \beta^2 \mathbf{u}_h^{(j)} \cdot \mathbf{v}_h \, ds - \int_{\Omega_t} p_h^{(j)} \nabla \cdot \mathbf{v}_h \, d\mathbf{x} = \rho \int_{\Omega_t} \mathbf{g} \cdot \mathbf{v}_h \, d\mathbf{x}, \\ - \int_{\Omega_t} q_h \nabla \cdot \mathbf{u}_h^{(j)} \, d\mathbf{x} = 0. \end{cases} \quad (5)$$

Finally, set $\mathbf{u}_h = \mathbf{u}_h^{(j)}$ when satisfactory convergence is achieved.

- It is robust with respect to the initial guess for the solution, but is at best *linearly convergent* for solving the nonlinear finite element Stokes system.
- It is time consuming for long-time and large-spatial scale simulations in practical applications, such as decades to century scale, whole-ice sheet simulations of Greenland and Antarctica.



Nolinear Solver: Newton Iterations

The Newton method is to seek $\delta \mathbf{u}_h$ and δp_h such that

$$\left\{ \begin{array}{l} \int_{\Omega_t} A^{-1/3} \epsilon_{\mathbf{u}_h^{(j-1)}}^{-2/3} \left(\dot{\epsilon}_{\delta \mathbf{u}_h} - \frac{2}{3} \frac{1}{(2\epsilon_{\mathbf{u}_h^{(j-1)}})^2} (\dot{\epsilon}_{\delta \mathbf{u}_h} : \dot{\epsilon}_{\mathbf{u}_h^{(j-1)}}) \dot{\epsilon}_{\mathbf{u}_h^{(j-1)}} \right) : \dot{\epsilon}_{\mathbf{v}_h} \, d\mathbf{x} \\ \quad + \int_{\Gamma_{b,slid}} \beta^2 \delta \mathbf{u}_h \cdot \mathbf{v}_h \, ds - \int_{\Omega_t} \delta p_h \nabla \cdot \mathbf{v}_h \, d\mathbf{x} = -\text{Res}_{\mathbf{u}}^{j-1}, \\ - \int_{\Omega_t} q_h \nabla \cdot \delta \mathbf{u}_h \, d\mathbf{x} = -\text{Res}_p^{j-1}. \end{array} \right. \quad (6)$$

where $\text{Res}_{\mathbf{u}}^{j-1}$ and Res_p^{j-1} are the residuals of (4) for the approximations \mathbf{u}_h^{j-1} and p_h^{j-1} , respectively. The approximate solution at the j th step of the Newton method is given by $\mathbf{u}_h^j = \mathbf{u}_h^{j-1} + \delta \mathbf{u}_h$ and $p_h^j = p_h^{j-1} + \delta p_h$.

- The diffusion part of the above variational problem is *coercive*.
- The Newton nonlinear iterative solver is *quadratically convergent* but are much less robust with respect to the initial solution guess.



Hybrid Picard-Newton Iterative Algorithm

- **Hybrid approach** [Leng et. al, *CiCP* 2014] – first run the Picard iteration for a few steps to provide a good initial guess for the Newton iteration, which then takes over until the solution converges. This approach provides a powerful and efficient tool for solving the nonlinear Stokes system.
- Both the Picard and Newton methods produce, at each step, the linear finite element problems respectively, which are symmetric saddle-point problems:

$$\begin{pmatrix} F & B^T \\ B & \mathbf{0} \end{pmatrix} \begin{pmatrix} \vec{u} \\ \vec{p} \end{pmatrix} = \begin{pmatrix} \vec{r} \\ 0 \end{pmatrix}. \quad (7)$$

- Efficient parallel linear system solvers based on MPI for (7) are developed in [Leng et. al, *JGR* 2012; Leng et. al, *CiCP* 2014].
 - Linear system solver: Domain Decomposition + FGMRES + Preconditioner (Additive Schwartz Method + Local Direct Solver)
 - The “PHG” (Parallel Hierarchical Grid) and “MUMPS” (MULTifrontal Massively Parallel Sparse direct solver) Packages.



FE Discretization of the Temperature Equation

- A few difficulties arise when solving the temperature equation:
 - The problem is advection-dominated in the horizontal directions,
 - The melting point constraint needs to be satisfied.
- Use the SUPG-FEM (Streamline Upwind Petrov-Galerkin Finite Element Method) to stabilize the numerical scheme: seek $T_h \in P_{3,h}(\mathcal{T}_h)$ satisfying $T_h|_{\Gamma_s} = T_{\text{surf},h}$

$$\begin{aligned}
 & \int_{\Omega_t} \left(\rho c \frac{\partial T_h}{\partial t} \phi_h + \rho c \mathbf{u}_h \cdot \nabla T_h \phi_h + \kappa \nabla T_h \cdot \nabla \phi_h + \mu \rho c (\mathbf{u}_h \cdot \nabla T_h) (\mathbf{u}_h \cdot \nabla \phi_h) \right) dx \\
 & = \int_{\Omega_t} 2\eta_{\mathbf{u}_h, T_h} \dot{\epsilon}_{\mathbf{u}_h} : \dot{\epsilon}_{\mathbf{u}_h} \phi_h dx
 \end{aligned} \tag{8}$$

for all $\phi_h \in P_{2,h}(\mathcal{T}_h)$ and $\phi_h|_{\Gamma_s} = 0$, where the stabilization parameter μ is set to be $\mu = h/(2\|\mathbf{u}_h\|_2)$ with h chosen locally as the diameter of the tetrahedron.



FV Discretization of the Ice Thickness Equation

- Let \mathcal{Q}_H denote the two-dimensional triangulation of the horizontal extent Ω_H of the ice-sheet. For each vertex v_i of \mathcal{Q}_H , we build a patch around v_i and then extend the two-dimensional patch in the vertical direction to create a volumetric patch P_i in the **layered** tetrahedral mesh \mathcal{T}_h .
- The explicit finite volume scheme for updating the ice thickness:

$$\frac{(H_i^{n+1} - H_i^n)S_i}{\Delta t} = \sum_j F_j^n + m_i S_i, \quad (9)$$

where H_i^n denotes the ice thickness at the vertex v_i at time t^n , $\{F_j^n\}$ is the set of fluxes at all lateral faces of the control volume P_i .

- The flux F^n is **upwinded** to stabilize the scheme in space; specifically,

$$F_j^n = \begin{cases} \bar{\mathbf{u}}_j \cdot \mathbf{n}_j l_j H_j^- & \text{if } \bar{\mathbf{u}}_j \cdot \mathbf{n}_j > 0 \\ \bar{\mathbf{u}}_j \cdot \mathbf{n}_j l_j H_j^+ & \text{otherwise,} \end{cases}$$

where l_j is the horizontal length of the j th lateral face, H_j^- is the average height inside the control volume, and H_j^+ is the average height in the neighboring control volume of the j th lateral face. 

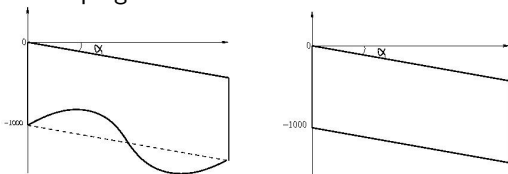


Outline

- 1 Background
- 2 Mathematical Modeling of Ice Sheet Flow
- 3 Computational Ice Sheet Model - Discretization and Solution
- 4 Numerical Experiments**
 - Tests of the Stokes ice dynamics solver
 - Tests of thermo-mechanically coupled ice sheet evolution
- 5 Conclusions

ISMIP-HOM Benchmark Test – Experimental Setup

- The ISMIP-HOM benchmark experiments focus on the diagnostic, 3D flow field within an idealized, predominantly rectangular slab of **isothermal** (the flow rate factor $A \equiv 10^{-16}$) ice with length L and average thickness 1 km, resting on a sloping surface.

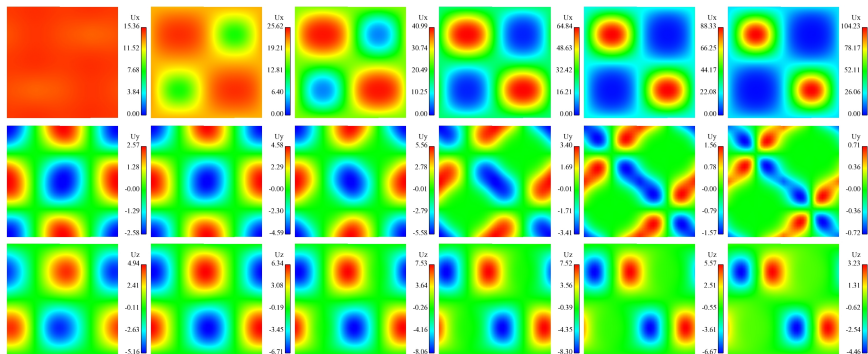


ISMIP-HOM Experiments A-B (Left) and C-D (right)

- Exps. A and B ($\alpha = 0.5^\circ$) have a zero-velocity Dirichlet BC on the basal surface.
- Exps. C and D ($\alpha = 0.1^\circ$) include a Rayleigh basal sliding BC with a periodic, specified pattern of the basal traction parameter β^2 .
- We conduct Exps. A-D on a $40 \times 40 \times 20$ structured tetrahedral grid (192,000 tetrahedral elements and 827,604 DOFs).



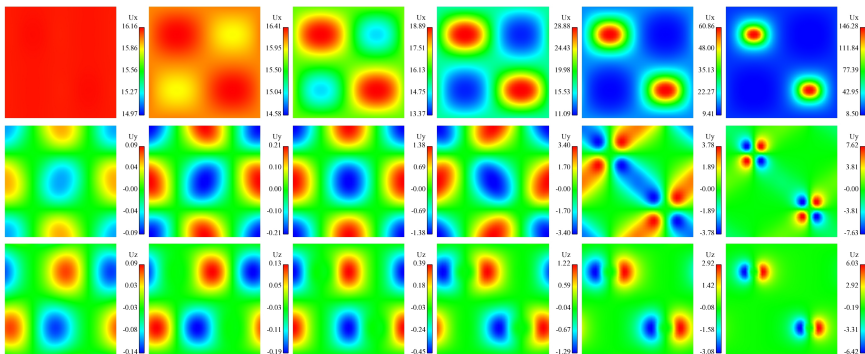
ISMIP-HOM Benchmark Test – Simulation Results of Exp. A



Simulation results at different length scales for Experiment A (Ice flow with no-slip). From top to bottom: the components u_1 , u_2 , and u_3 of the top surface velocity ($m a^{-1}$); from left to right: $L = 5, 10, 20, 40, 80, 160$ km.



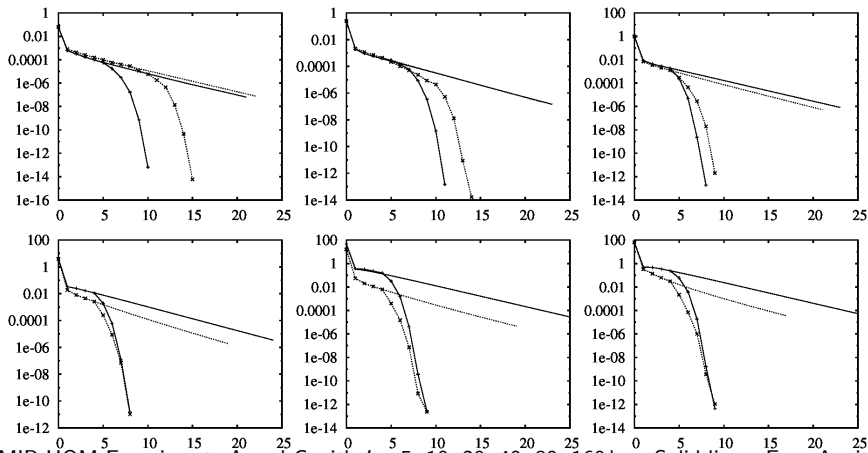
ISMIP-HOM Benchmark Test – Simulation Results of Exp. C



Simulation results at different length scales for Experiment C (Ice flow with basal slip). From top to bottom: the components u_1 , u_2 , and u_3 of the top surface velocity ($m a^{-1}$); from left to right: $L = 5, 10, 20, 40, 80, 160$ km.



ISMIP-HOM Benchmark Test – Picard vs. Hybrid Methods



ISMIP-HOM Experiments A and C with $L=5, 10, 20, 40, 80, 160$ km. Solid lines: Exp. A with Picard method. Solid lines with asterisk: Exp. A with Picard-Newton method. Dashed lines: Exp. C with Picard method. Dashed lines with plus: Exp. C with Picard-Newton method.



Analytic Solution Test – 3D Stokes Solution Construction

- An idealized rectangular slab of isothermal ice sheet with length L and average thickness $Z = 1$ km, resting on a sloping surface with a mean slope of $\alpha = 0.5^\circ$. Let $s_0(x, y) = -x \tan(\alpha)$.
- The fixed smooth basal topography is defined as a series of 500m amplitude sinusoidal oscillations about the mean bed elevation:

$$b(x, y) = s_0(x, y) + \eta(x, y) - Z.$$

with $\eta(x, y) = \frac{Z}{2} \sin\left(\frac{2\pi x}{L}\right) \sin\left(\frac{2\pi y}{L}\right)$.

- Due to ice sheet flow and accumulation at the surface, the top surface of the ice sheet slowly evolves from flat with a uniform slope to sinusoidal in shape:

$$s(x, y, t) = s_0(x, y) + \eta(x, y)\xi(t)$$

with $\xi(t) = 1 - e^{-c_t t}$ where c_t is a parameter that controls the rate of ice thickness change.

- No-slip boundary condition is applied at the bottom surface, and periodic boundary condition is applied at the lateral surface.



Analytic Solution Test – 3D Stokes Solution Construction

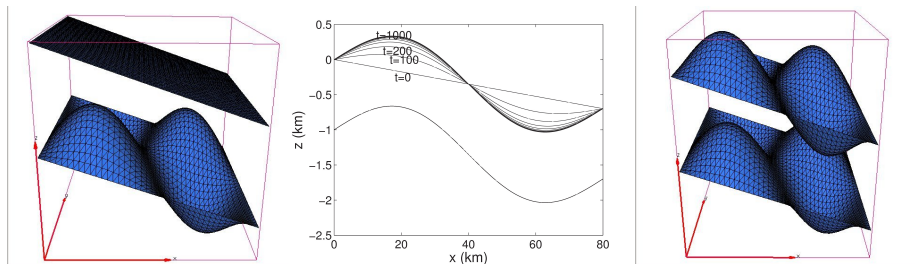


Illustration of the ice-sheet geometry (the top and bottom surfaces) at the time $t = 0$ (left) and at the time $t = 1000$ years (right). The middle figure is the x -direction profiles taken at $y = L/4$ of the ice-sheet top and bottom surfaces at 100 year time intervals from $t = 0$ to 1000 years.



Analytic Solution Tests – 3D Stokes Solution Construction

- A manufactured solution satisfies the compensated Stokes equation and the boundary conditions is then given by [Leng et. al, *The Cryosphere* 2013]:

$$\begin{aligned}
 u(x, y, z, t) &= c_1 \left[1 - \left(\frac{s-z}{s-b} \right)^4 \right], \\
 v(x, y, z, t) &= \frac{c_2}{s-b} \left[1 - \left(\frac{s-z}{s-b} \right)^4 \right] \\
 &\quad - \frac{1}{2} \frac{c_1}{s-b} \left[1 - \left(\frac{s-z}{s-b} \right)^4 \right] Z \cos\left(\frac{2\pi x}{L}\right) \cos\left(\frac{2\pi y}{L}\right) e^{-c_2 t}, \\
 w(x, y, z, t) &= u(x, y, z, t) \left(\frac{\partial b}{\partial x} \frac{s-z}{s-b} + \frac{\partial s}{\partial x} \frac{z-b}{s-b} \right) \\
 &\quad + v(x, y, z, t) \left(\frac{\partial b}{\partial y} \frac{s-z}{s-b} + \frac{\partial s}{\partial y} \frac{z-b}{s-b} \right).
 \end{aligned}$$

and

$$p(x, y, z, t) = -2\eta_u \frac{\partial u}{\partial x} - 2\eta_u \frac{\partial v}{\partial y} + \rho g(s-z).$$

where c_1 and c_2 are parameters to control the velocity falling within a reasonable range.



Analytic Solution Test – Ice Sheet Dynamics: T-H vs. Enriched T-H

Convergence and local mass conservation comparisons:

The enriched T-H model at the initial state $t = 0$

Mesh	Velo. Error	Conv. Rate	Pres. Error	Conv. Rate	$\max \text{div}(\mathbf{u}) $
$20 \times 20 \times 5$	5.53×10^0	-	5.46×10^{-1}	-	6.71×10^{-9}
$40 \times 40 \times 10$	7.77×10^{-1}	2.83	1.80×10^{-1}	1.59	3.44×10^{-10}
$80 \times 80 \times 20$	1.53×10^{-1}	2.34	5.67×10^{-2}	1.67	5.89×10^{-10}
$160 \times 160 \times 40$	3.57×10^{-2}	2.16	1.66×10^{-2}	1.77	1.17×10^{-10}

The T-H model at the initial state $t = 0$

Mesh	Velo. Error	Conv. Rate	Pres. Error	Conv. Rate	$\max \text{div}(\mathbf{u}) $
$20 \times 20 \times 5$	6.21×10^0	-	5.34×10^{-1}	-	1.04×10^{-4}
$40 \times 40 \times 10$	6.26×10^{-1}	3.40	1.79×10^{-1}	1.62	2.19×10^{-4}
$80 \times 80 \times 20$	6.69×10^{-2}	3.33	5.62×10^{-2}	1.66	1.11×10^{-4}
$160 \times 160 \times 40$	8.49×10^{-3}	3.22	1.64×10^{-2}	1.70	5.59×10^{-5}



Analytic Solution Test – Parallel Scalability: T-H vs. Enriched T-H

Running time and weak scalability comparisons (the cluster “Hopper” at NERSC):

Weak scalability for the enriched T-H model

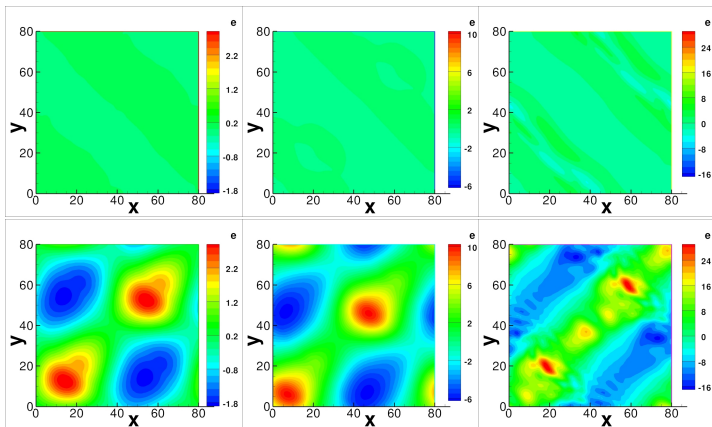
Mesh Size	DOFs	Number of Procs	NOIs-nonlinear	Total Time (sec)	Scalability S_{weak}
$20 \times 20 \times 20$	253,200	16	8	152	-
$40 \times 40 \times 20$	1,012,800	64	8	228	0.67
$80 \times 80 \times 20$	4,051,200	256	8	270	0.56
$160 \times 160 \times 20$	16,204,800	1024	8	356	0.43

Weak scalability for the T-H model

Mesh Size	DOFs	Number of Procs	NOIs-nonlinear	Total Time (sec)	Scalability S_{weak}
$20 \times 20 \times 20$	205,200	16	8	117	-
$40 \times 40 \times 20$	820,800	64	8	159	0.73
$80 \times 80 \times 20$	3,283,200	256	8	206	0.57
$160 \times 160 \times 20$	13,132,800	1024	8	298	0.39



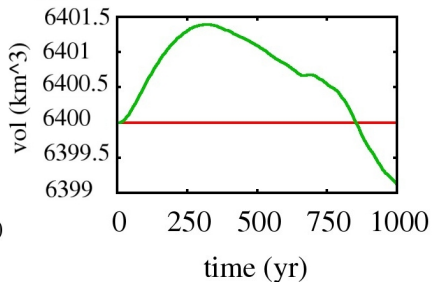
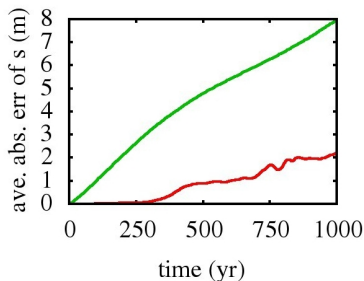
Analytic Solution Test – Thickness Evolution: T-H vs. Enriched T-H



Distribution of the errors of the simulated top surface elevation (m) by the the enriched T-H element model (top) and the T-H element model (bottom) for the time-dependent ice-sheet flow experiment. From left to right: at 100, 300, and 1,000 years.



Analytic Solution Test – Thickness Evolution: T-H vs. Enriched T-H



Plot of the average absolute errors (left) of the simulated top surface elevation s (m) and the total volume (right) of the ice sheet at each of the time steps for the time-dependent ice-sheet flow experiment using the grid of resolution $80 \times 80 \times 20$ and a time step size of 2 years. Red: the enriched T-H element model; green: the T-H element model.

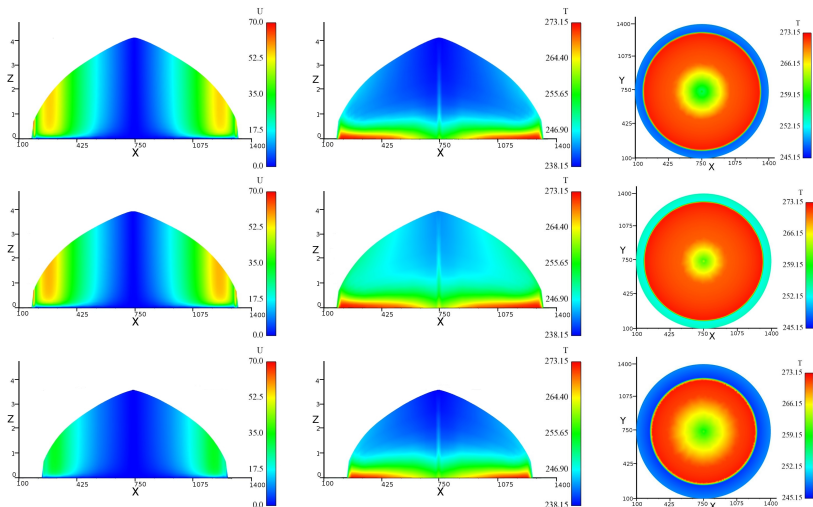


EISMINT-II Benchmark Test – Overview

- The European Ice-Sheet Modeling Initiative (EISMINT) consists of a series of idealized prognostic experiments for studying the behavior of models designed to simulate ice-sheet evolution.
- The second phase of that set of experiments, EISMINT-II, focused on thermo-mechanically coupled ice-flow evolution.
 - Feature a square domain $[0, 1500\text{km}]^2$;
 - Assume a radially symmetric ice-sheet geometry and boundary conditions with radially symmetric and idealized climate forcing – ice accumulation rate M , the circle of radius R_{el} , ice-sheet surface temperature T_{surf} , etc.;
 - Depending on the experiment, no-slip or sliding basal boundary conditions are prescribed.
- While all SIA-based models tested showed considerable agreement in their predictions,
 - Symmetry is often broken and distinct, regularly spaced “cold-ice spokes” appear.



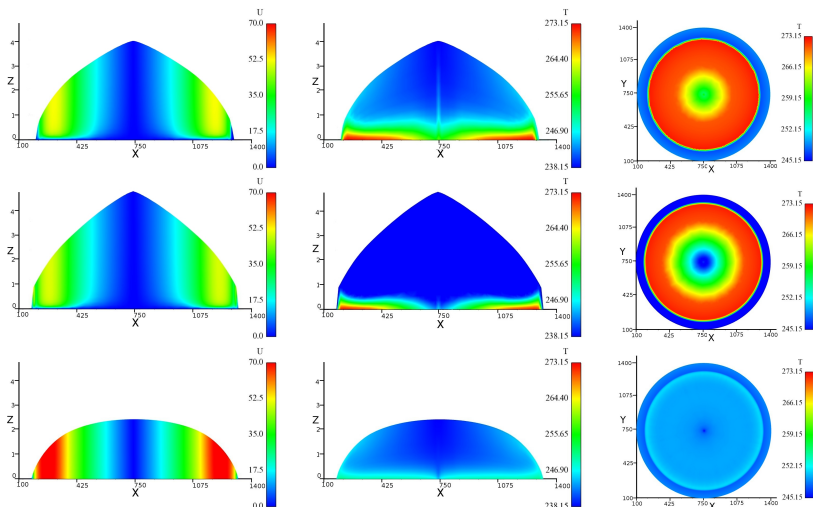
EISMINT-II Benchmark Test – Steady State of Exps. A, B, C



From left to right: the velocity magnitude on the xz -plane, the temperature (K) on the xz -plane, and the basal temperature on the xy -plane. From top to bottom: Exps. A, B, C.



EISMINT-II Benchmark Test – Steady State of Exps. D, F, G

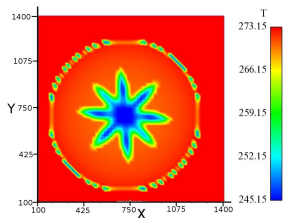


From left to right: the velocity magnitude on the xz -plane, the temperature (K) on the xz -plane, and the basal temperature on the xy -plane.

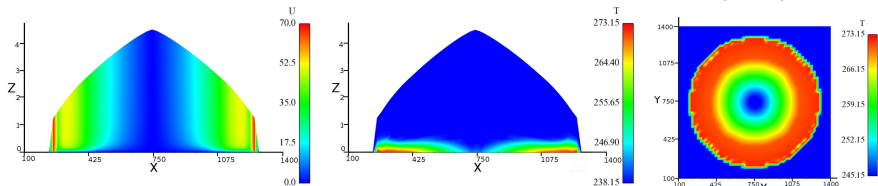


On the Cold Spoke Instability – What cause it?

Simulation results of basal temperature on the xy -plane of steady states of the EISMINT-II Exp. F on the structured grid $60 \times 60 \times 10$ [Leng et. al, 2014]



By the SIA ice dynamical core in the Community Ice Sheet Model (CISM)



By our parallel computational 3D Stokes ice sheet model



Outline

- 1 Background
- 2 Mathematical Modeling of Ice Sheet Flow
- 3 Computational Ice Sheet Model - Discretization and Solution
- 4 Numerical Experiments
 - Tests of the Stokes ice dynamics solver
 - Tests of thermo-mechanically coupled ice sheet evolution
- 5 Conclusions



Concluding Remarks

- We have developed “FELIX- Stokes” – a parallel computational model of higher-order discretization accuracy and variable grid resolution capability for simulating the 3D, thermo-mechanical behavior of ice sheets.
 - The nonlinear Stokes equations are solved using a hybrid Picard-Newton solver, which reduces the number of iterations needed for convergence significantly when compared to the Picard solver alone.
 - The enriched Taylor-Hood finite element greatly enhances local mass conservation over the classic one for the ice sheet dynamics modeling.
 - The thermomechanically coupled model can be applied to large-scale problems, and is physically reliable over very long time integrations.
 - When applying our model to the EISMINT-II experiments for ice sheet evolution, we find no evidence for the cold spoke instabilities seen by using lower-order approximations.

